The effect of CO_2 on the speciation of RbBr in solution at temperatures to 579°C and pressures to 0.26 GPa

Evans, K.A.[*], Gordon, R.A. [†], Mavrogenes, J.A. [‡], Tailby, N [‡].

February 11, 2009

[*]RSES, ANU, ACT 0200, Australia; now at Dept. Applied Geology, Curtin University, GPO Box U1987, Bentley, WA6845, Australia

[†]PNC-CAT, APS, Argonne National Laboratory, 9700 South Cass Avenue - Building 460 Argonne, IL 60439, USA

[‡]RSES, ANU, ACT 0200, Australia

1 ABSTRACT

Carbon dioxide- and salt-bearing solutions are common in granulite, ore-forming and magmatic environments. The presence of CO_2 affects mineral solubilities, fluid miscibility, and viscosity and wetting properties, and is expected to affect salt speciation. EXAFS measurements of RbBr-H_2O-CO_2 fluids contained in corundum-hosted synthetic fluid inclusions (SFLINCs) have been used to investigate the effect of CO_2 on salt speciation at temperatures to 579°C and pressures to around 0.26 GPa.

Forward modelling indicates that solute dehydration is difficult to distinguish from up to around 40% of Rb-Br ion-pairing, so results refer to the total number of nearest neighbours, which are likely to be mostly O present in waters of hydration, but may also include Br, if ion pairing is present. Additionally, results relate to the number of well-ordered neighbours in the first shell, because nearest neighbours with a high degree of disorder may be present but contribute minimally to the EXAFS signal. Analysis of the EXAFS results at the Rb edge for the CO_2-free solution is consistent with previous work and shows that the number of nearest neighbours for Rb in CO_2-free solutions decreases from 6 $\pm$0.6 to 1.4 $\pm$0.1 as temperature increases from 20°C to 534°C. The decrease is accompanied by a decrease in Rb-x bondlengths of 0.05 Å, where x is the first shell scatterer. Results for the CO_2-bearing solution are different to those for the CO_2-free solution. The number of nearest neighbours is 16 and 22% less than for the CO_2-bearing solution at 312 and 445°C respectively. Changes in the numbers of nearest neighbours correlate well with calculated changes in the bulk solution dielectric constant; CO_2-bearing and CO_2-free solutions lie on the same trend, which suggests that it may be possible to calculate the number of nearest neighbours from dielectric constant. Rb-x bondlengths for the CO_2-bearing solution are statistically indistinguishable to those for the CO_2-free inclusions. Results for Br are worse quality than for Rb so EXAFS analysis could not be completed, however XANES spectra for CO_2-free and CO_2-bearing solutions are consistent with solute dehydration similar to that recorded by the Rb spectra. The conclusions of this study provide support for the notion that CO_2 has a fundamental effect on the mechanics of solubility, and that these effects should be incorporated into conceptual

and quantitative thermodynamic models.

2 INTRODUCTION

Carbon dioxide and a range of salts that include NaCl, KCl and $CaCl_2$ are constituents of geological solutions involved in the formation of gold and other ore deposits (e.g. Phillips and Powell, 1993; Phillips and Evans, 2004), granulite metamorphism (e.g. Newton et al., 1998), mafic, intermediate and felsic magmatism (e.g. Baker, 2002; Caracausi et al., 2005; Thebaud et al., 2006), carbonate metamorphism (e.g. Ferry, 1994) and seafloor hydrothermal alteration (e.g. Butterfield et al., 1994). The presence of salts and CO_2 affects physical and chemical properties of solutions that include miscibility characteristics (e.g. Shmulovich and Graham, 1999), mineral solubility (e.g. Newton and Manning, 2000; Shmulovich et al. 2001), viscosity and wetting properties (e.g. Holness and Graham, 1995; Wark and Watson, 2002).

One reason for these effects is that CO_2 is less polar than water, so CO_2 in solution reduces hydrogen bonding and reduces the dielectric constant. Dielectric constant measures the ability of a solution to store electrical energy, and, practically, indicates the ability of the solvent to screen the charge of ions in solution and form hydrated solute complexes. Dielectric constant is related to mineral solubility; ionic substances dissolve readily in high dielectric constant solutions, while organic substances are more soluble in low dielectric constant solutions. For most terrestrial geotherms, the dielectric constant decreases with increasing temperature at constant pressure, and increases with pressure at constant temperature (e.g. Helgeson and Kirkham, 1974). Decreases in dielectric constant promote ion-pairing and complex formation. The addition of CO_2 to solutions would be expected to cause similar effects, although these have not yet been demonstrated.

X-ray Absorption Fine Structure (XAFS) utilises synchrotron radiation to obtain information on atomic environments within an analysed material, and can be used to determine solute speciation (e.g. Pfund et al., 1994, Fulton et al., 1996; Seward et al., 1999). Synchrotron radiation provides intense X-rays that can be tuned accurately to a specified energy, and focussed on the micron scale. An XAFS spectra comprises measurements of the absorption of a sample, in this case, a solution, as a function of incident X-ray energy as the energy is scanned across the absorption edge of the element of interest. Extended X-ray Absorption

Fine Structure (EXAFS) spectra extend from a 10-30 eV above the absorption edge to a few 100s of eV above the edge, and are the object of interest here. EXAFS studies of solutes in fluids have been used to deduce the numbers and identities of nearest neighbours and nearest neighbour distances (e.g. Pfund et al., 1994; Fulton et al., 1996; Mayanovic et al., 2001; Simonet et al., 2002).

It would be most useful to acquire EXAFS measurements on NaCl, the most common salt in geological solutions. However, the low atomic numbers of Na and Cl mean that information on this salt can only be obtained from relatively low energy X-rays, which are almost entirely absorbed by the experimental apparatus required to contain high pressure-temperature fluids. For this reason a number of studies have focussed on RbBr (e.g. Fulton et al., 1996; Newville et al., 1997; Wallen et al., 1997; Ferlat et al., 2001; Ferlat et al., 2002) because the absorption edges of Rb and Br are at sufficiently high energy (13 - 16 KeV), that the X-rays of interest pass through experimental apparatus without excessive absorption. RbBr is similar to NaCl in that it is a cubic ionic compound of group I and group VII ions. Both are highly soluble and dissociate fully in aqueous solutions at room temperature, and the ratio between charge and ionic radius is similar. The behaviour of RbBr is therefore likely to have some similarities to that of NaCl.

Previous EXAFS measurements of RbBr solutions at elevated pressure and temperature (e.g. Fulton et al., 1996; Newville et al., 1997; Wallen et al., 1997; Ferlat et al. 2001) show a reduction in the amplitude of the XAFS signal as pressure and temperature increase. Most studies have attributed this feature to a reduction in the number of waters of hydration (Fulton et al., 1996; Newville et al., 1997; Wallen et al., 1997). However, Ferlat et al. (2001) proposed that the signal reduction is due to local fluctuations in the number and location of solvated waters, without any change in the total number of solvated waters. No conclusive evidence of any other changes in RbBr speciation with increasing temperature and pressure have been found, although molecular dynamics (MD) simulations (e.g. Wallen et al., 1997; Ferlat et al., 2001) suggest that ion-pairing should occur, and studies of $ZnCl_2$ and $ZnBr_2$ in Na-halide solutions have revealed ion pairing and other complexes, such as $ZnCl_4^{2-}$ (Mayanovic et al., 1999; Mayanovic et al., 2001; Simonet et al., 2002).

Speciation in solutions that contain both salt and CO_2 has not, as yet, been investigated with EXAFS although CO_2 might be expected to affect speciation given its effect on dielectric constant. One reason for this omission is the difficulty of experiments that involve CO_2; CO_2 is sparingly soluble in water at room temperature and pressure, and this results in limited experimental access to CO_2-rich fluid compositions. In this study CO_2-rich solutions at temperatures, pressures and densities of geological interest are investigated using synthetic fluid inclusions (SFLINCs: e.g. Shelton and Orville, 1980; Sterner and Bodnar, 1984; Frost and Wood, 1997). XANES (X-ray absorption near-edge spectra) and SXRF (synchrotron X-ray fluorescence) measurements have previously been made successfully on natural and synthetic fluid inclusions (e.g. Mavrogenes et al., 1995; Mavrogenes et al., 2002; Thebaud et al., 2006; Evans et al., 2007) but EXAFS, which requires higher signal:noise ratios than the other techniques, has so far proved difficult. In this study, EXAFS measurements of RbBr in corundum-hosted CO_2-bearing and CO_2-free SFLINCs are compared, and CO_2-induced changes in salt speciation are discussed.

3 METHODS

<begin small type>

Synthetic corundum was cut and ground into 3 mm diameter cylinders, which were heated to 1100°C in a muffle furnace and quenched in water. This process created a fine network of fractures which act as hosts of the SFLINCs. Corundum was used for this study because its strength allows high internal pressures (up to 1 GPa) without alteration or destruction of the SFLINCs (Frost and Wood, 1997). For most of the experiments the corundum was loaded into 9 mm diameter swaged silver capsules with weighed quantities of ultra-pure RbBr (Sigma-Aldrich), silver oxalate ($Ag_2C_2O_4$), deionised water, and a small quantity of Al_2O_3 powder. The purpose of the latter was to aid healing of the fractures via provision of a source of metastable Al_2O_3. Fluid compositions with $X(CO_2)$ between 0 and 0.15 were investigated; these compositions fall within the range found in common geological

environments (e.g. Ferry, 1994; Phillips and Evans, 2004). A small number of experiments utilised 5mm Pt tubing because higher temperatures can be used for Pt-hosted experiments, and it was thought that these high temperatures might be necessary to produce high quality SFLINCs in corundum.

Silver oxalate was made fresh for this study and yields were checked by heating weighed quantities in sealed Pt tubing to 300°C. The tubes were weighed, pierced and reweighed. The mass of CO_2 evolved from the silver oxalate was calculated and compared with the theoretical value. Yields were within error of 100%. It was intended that the fluids would lie within the one fluid phase field at the pressure and temperature of SFLINC synthesis. Phase relations for the system H_2O-CO_2-RbBr are not well known at the pressures and temperatures of interest, so suitable conditions were estimated by comparison with the phase diagram for H_2O-CO_2-NaCl (Shumulovich et al., 1999) and with the web-based GeoFluids software (http://geotherm.ucsd.edu) which utilises the Duan et al. (1995, 2003) Equation of State (EOS) for H_2O-CO_2-NaCl. All results were corrected to account for the mass of RbBr. The density of the fluid within the capsule was approximately 0.8 g cm^{-3}. Capsules were run in the piston cylinder apparatus at the Research School of Earth Sciences at the Australian National University. The Ag capsules were run at 800°C and 0.8 GPa and the Pt capsules were run at 900°C and 0.8 GPa. Both types of capsule were run for three days before quenching.

After each run the capsules were pierced and the corundum extracted. Only corundum from capsules that released fluid during piercing were utilised for this study, as this indicates that fluids were retained throughout the experiment. The corundum pieces were set in EPO-FIX epoxy and double polished to about 1mm thickness. The samples were extracted from the epoxy and characterised optically. The positions of shallow inclusions that lie less than 50 microns beneath the crystal surface were noted, as previous investigations (Evans et al., 2007) have shown that this is the maximum depth for which a good XAFS signal can be obtained. Two samples were selected for EXAFS analysis. These were a CO_2-free sample, COR 2, with a mole fraction of RbBr, X(RbBr), of around 0.05, and a CO_2-bearing sample, COR 5, with X(CO_2) of around 0.1, and X(RbBr) close to 0.06. Fluid compositions

are defined in terms of $X(CO_2)$ and X(RbBr) where X refers to the mole fraction of each component. Mole fractions were calculated, for convenience, assuming that the salt, water and CO_2 remain associated. The veracity of this assumption does not affect the conclusions of this study.

XAFS measurements were made at the microprobe end-station (Heald et al., 2001) on beamline 20-ID at the Advanced Photon Source (APS). The energy of incident radiation was controlled with a Si(111) double crystal monochromator with an energy resolution of $\Delta E/E$ of 10^{-4}. The monochromator was slightly detuned to enhance harmonic rejection. All samples, including the standards, were measured in fluorescence geometry. The fluorescent signal was detected with a 7 element Canberra Ge(Li) detector. Standards measured included RbBr powder, 0.1m, 1m, and 6m RbBr solutions, and RbBr in $NaHCO_3$, K_2CO_3 and Na_2CO_3 solutions. A solid RbBr sample mounted on tape was continuously measured during the run, to monitor the monochromator energy calibration. No significant drift occurred over the course of the 48 hour run. The samples were loaded onto a high temperature LINKAM TS1500 heating stage, which was fixed vertically at a 45° angle to the X-ray beam. The beam was defocussed to around 30 x 30 microns to minimise effects of bubble movement within inclusions, and to reduce the probability of beam damage to the inclusions. A calibration of the temperature at the surface of the sample against the temperature recorded by the stage was made after the run using an independent thermocouple. This showed a linear relationship between stage temperature and recorded temperature that fit to the expression $T_{\mathrm{crystal}} = 0.89 T_{\mathrm{stage}}$.

Inclusions were located optically, a process that was aided by bright blue fluorescence of the corundum in the path of the X-ray beam. The precise location for which the maximum signal could be obtained was determined using 2D mapping. XAFS scans were made across the Rb and Br edges, from 200 eV below the edge to 600 eV above the edge. 10 scans were made at each temperature. Each scan took about 20 minutes. The SFLINCs were remapped after each temperature increase because thermal expansion caused small movements of the inclusion relative to the beam. The Rb signal from the Canberra detector was normalised against the Br signal, to remove the effects of small scale sample movement, and, at temper-

atures below the critical temperature, effects of bubble movement within inclusions. Spectra were taken at room temperature, and at indicated temperatures of 100°C, 200°C, 350°C, 500°C, 600°C and 650°C. Actual temperatures, according to the temperature calibration, were 89°C, 178°C, 312°C, 445°C, 534°C, and 579°C respectively. At temperatures less than the homogenisation temperature of 385°C, X(CO_2) in the liquid part of the SFLINCS would have been less than the bulk mole fraction because CO_2 partitions strongly into the vapour phase. RbBr partitions into the liquid, which therefore provides the XAFS signal. X(CO_2) in the measured solution would have been < 2 mole % at room temperature and increased as the the homogenisation temperature was approached; precise measurements of the X(CO_2) at each temperature are impossible because of poorly known P-V-T relationships in the H_2O-CO_2-RbBr system. The inclusions were inspected after the run for signs of damage and stretching.

Microthermometric observations were made post-run (Table 1) to check the composition of fluids in inclusions. Samples were heated and cooled on a Fluid-Inc United States Geological Survey heating-freezing stage. The accuracy of the temperature measured by the stage thermocouples for the relatively thick samples was checked using the first melting point for CO_2 and was found to be within $\pm$ 2°C of the correct value. Temperatures of first and final melting, CO_2-homogenisation, and total homogenisation were recorded for five to seven inclusions from each sample. Interpretation of microthermometry to obtain rough estimates of X(CO_2) and X(salt) was performed using the program MacFlincCOR (Brown and Hagemann, 1995), which calculates fluid composition for H_2O-CO_2-NaCl fluids based on the EOS of Bowers and Helgeson (1985), for CO_2-free inclusions, and Brown and Lamb (1989), for CO_2-bearing inclusions. Pressures at the run temperatures were estimated with the web-based GeoFluids software (http://geotherm.ucsd.edu), as described above. Results are approximate because these EOS are for NaCl-bearing systems rather than RbBr, and, in the case of the MacFlincCOR EOS, are calibrated for lower pressures than those of interest here.

Post-run, the scans were inspected and poor quality scans were rejected. The remaining scans at each temperature were averaged and the background subtracted using the AutoBk

routine (Newville, 2001) which is embedded in the Athena software (Ravel and Newville, 2005). R_{bkg}, which specifies the minimum distance for which information is provided by the signal, was increased to 1.4 remove low R artefacts from the signal. This strategy did not significantly affect the fit parameters. EXAFS interference functions, chi(k), multiplied by k^2 to increase the signal at high k values, were exported into Artemis (Ravel and Newville, 2005). These data were Fourier-transformed via a Hanning window with a dk of 2, and fit to the EXAFS equation (e.g. Fulton et al., 1996). The theory used for the EXAFS fit was a first shell approximation of octahedrally co-ordinated Rb with six oxygens at a distance of 2.93 Å. This distance was taken from the results of Fulton et al. (1996). The applicability of the first shell approximation (QFS) was tested by a comparison of the results to fits to the first ten paths from a full FEFF6 calculation based on the parameters for Rb_2O from Wyckoff (1963). A tetrahedral geometry for the first shell was also tested.

The EXAFS equation was fit for the product of the nearest neighbour oxygens (n) and the amplitude reduction term (S_0^2), the difference between the initial model nearest neighbour distance and the real distance (Δr), the mean-square-relative-displacement (σ^2), which measures the degree of disorder present in the signal, and the third cumulant, $c3$, which measures the asymmetry in the signal disorder. The edge energy for Rb, E_0, which is often used as a fitting parameter in this type of work (e.g. Fulton et al., 1996) was set to value that gave a Δr of 0 for room temperature, which was -6.6 eV for COR 2, and -5.4 eV for COR 5. These values of E_0 lie on the main absorption edge. This strategy was employed because the Rb edge energy was highly correlated with Δr and uncertainties on Δr became unreasonably large when E_0 was allowed to vary freely. Fitting was also performed with the spectra weighted by a combination of k and k^2, in an attempt to break the correlations between the fit parameters. The best results were obtained for a Fourier filtered k-range of 2.5 to 6.5 $\mathring{A}^{-1}$, and a fit R-range of 1.5 to 3.5 $\mathring{A}$; equivalent results were obtained for alternative fits that used an R range of 1.0 to 3.5 $\mathring{A}$ to investigate the effect of using a fit range that included R values less than R_{bkg}. Reported uncertainties were obtained from two different sources; first, from the one standard deviation reported by Artemis, which includes the effects of correlation between the fit variables, and second, calculated from the values

that cause a doubling of the sum of squares from the minimum value (c.f. Gordon et al., 2000); this method examines the stability of the fit with respect to variations in a given parameter.

Alternative fitting strategies were also applied to investigate the effects of correlations between the parameters and determine the degree of model-dependence of the fit parameters. For example, σ^2 was set to 0.03, a value comparable to values for this study and by other workers (e.g. Fulton et al., 1996; Simonet et al., 2002), while the other three parameters (n, Δr, and $c3$) allowed to vary, the maximum σ^2 was found for an R factor value of less than 0.05, and $c3$ was set to zero while n, Δr, and the Rb edge energy were allowed to vary. Fits were considered successful when the R-factor of the fit was less than 0.05, and the fit parameters passed simple reality checks; n, S_0^2, and σ^2 were not allowed to be negative. n was calculated under the assumption that S_0^2 was 0.98, a value derived for Rb by Frenkel et al. (1993).

Forward models were also run to investigate the effects of contact ion-pairs on the spectra. These models involve combination of the results from two QFS models for which all the parameters were set to the values of interest. The first model has oxygen nearest neighbours to mimic hydrated ions and the second has Br nearest neighbours, to mimic ion pairing. σ^2 was set to 0.03 (e.g. Fulton et al., 1996; Simonet et al., 2002). An estimate on the lower limit of proportion of Rb-Br pairing that would be detectable via EXAFS was made by fitting the theoretical chi(k) spectra to an octahedral Rb-O theory.

<end small type>

4 RESULTS

4.1 Fluid inclusion characteristics

Optical inspection of the corundum revealed abundant, regularly shaped fluid inclusions of moderate size (10 - 20 micron) (Fig. 1). The quality of SFLINCs was superior for the Ag-capsule-hosted runs in that the inclusions were more abundant, showed more regular shapes, and were less inclined to deform during heating. This can be seen in Fig. 1a and c, which compares SFLINCS from COR 2, which was from a Pt capsule, to SFLINCS from COR 5 which is from an Ag capsule.

Inclusions in the CO_2-free sample, COR 2, were crystal-free. Inclusions in the CO_2-bearing sample, COR 5, have double bubbles which is consistent with the presence of CO_2, as CO_2 is present as immiscible vapour and liquid phases. Rounded translucent crystals less than one micron in diameter could be seen in some of the inclusions in the CO_2-bearing sample, COR 5. The small size of these crystals means that they would only be visible if they were in a favourable orientation relative to the inclusion walls, so the apparent lack of crystals in all inclusions does not necessarily mean that fluid compositions in COR 5 were heterogeneous. Indeed the lack of variation in inclusion homogenisation temperature for this sample (Table 1) suggests that inclusion compositions were, in fact, homogeneous. RbBr is soluble at room temperature at the concentrations measured in the fluid inclusions so the crystals are unlikely to be RbBr. An alternative possibility is AgBr, with Ag sourced from the walls of the experimental capsule, and if this is the case then AgBr complexes could have caused artefacts in the experimental results. The solubility of AgBr as a function of temperature up to 368K is given by Zelyanskii et al. (2001). Their expression was extrapolated to 534°C to obtain an estimate of possible Ag concentrations at this temperature. Calculated Ag concentrations were 0.009 moles litre^{-1} at 534°C, which is about 3% of the calculated RbBr concentrations of 2.92 moles litre^{-1}. The volume of AgBr crystals necessary to give an molal Ag concentration of 10% of the Rb concentration was also calculated as a cross check on this result, under the assumption that a Ag:Rb ratio smaller than 0.1 would be unlikely to cause

result in a visible Ag-Br contribution to the XAFS spectra. The calculated volume for an inclusion of 20μm diameter is 68 μm^3, which is far in excess of any observed quantity. Thus, Ag concentrations were never greater than 10% of the Rb concentration and it is highly improbable that AgBr complexes affected the EXAFS.

Characterisation of the fluid inclusions by microthermometry (Table 1) indicates that the composition of the fluid inclusions is close to the intended composition. COR 2 shows some variation in homogenisation temperature; one large inclusion, marked X in Fig. 1c, homogenises at a higher temperature than the other smaller inclusions. This inclusion was not included in the XAFS study or subsequent analysis. The average total homogenisation temperature was 385 °C for both COR 2 and COR 5, so measurements made at 445, 534 and 579°C are all in the supercritical field. Exposure to the synchrotron X-ray beam at elevated temperature caused some damage to the inclusions (Figs 1c, d). The walls of the inclusions became less smooth, the double nature of the CO_2-bubble became more pronounced, the size of the crystals at room temperature increased, and inclusions very near to the crystal surface decrepitated. Such changes are consistent with small changes in inclusion volume during the run, but progressive changes in X-ray spectra were not seen over the course of acquisition of multiple spectra at each temperature, so the small changes to the visible appearance of the inclusions are thought not to have affected the EXAFS. Measurements of inclusion dimensions were made in an attempt to constrain the magnitude of possible density changes as a result of inclusion volume changes. The size of the changes could not be resolved, i.e. it was less than 1 micron in inclusion dimensions. The propagated density change from a change in inclusion dimensions of 1 micron is ± 15 % so the actual density change must have been less than this value.

4.2 Rb XAFS

The Rb EXAFS spectra (Fig. 2) are sufficient quality to derive first shell information, which supports the viability of SFLINCs for EXAFS studies. Chi(k) spectra show well defined oscillations up to a k value of 6.5 to 7 for COR 2 and COR 5 (Figs 2a,b). The amplitude of

the oscillations decreases significantly with temperature, and the period increases slightly. The non-phase corrected Fourier Transform of the spectra shows a well defined peak at around 1.8 Å for both COR 2 and COR 5 (Figs 2c,d). The amplitude of the peak decreases with increasing temperature and the maxima moves to slightly lower R values. The spectra fit well to the EXAFS theory (Fig. 3, Table 2). Results from the QFS theory and full Feff6 calculations were indistinguishable, as were results with different assumed geometry.

Consensual agreement between the different fit strategies employed was obtained for a qualitative decrease in co-ordination number, n, with increasing temperature. The presented fit results (Fig. 4, Table 2) refer to those for a Fourier filtered k-range of 2.5 to 6.5 $\mathring{A}^{-1}$, and a fit R-range of 1.5 to 3.5 $\mathring{A}$, and freely varying σ^2. The first shell co-ordination number, n, decreased with increasing temperature, from around 6 at room temperature and pressure, to 1.4 at temperatures of 534 or 579°C. Fit Rb-scatterer distances decreased by 0.05 $\mathring{A}$ for COR 2 between room temperature and 534 °C. Rb-scatterer distances for COR 5 apparently increased slightly then decreased between ambient temperature and 579°C, although uncertainties on these distances were sufficiently large that trends are unreliable (Fig. 4b). The number of nearest neighbours was consistently lower for the CO_2-bearing inclusions than for the CO_2-free inclusions, although the difference was not statistically significant if the Artemis-derived uncertainties were used. If the smaller uncertainties from Gordon et al. (2000), which omit corrrelation effects, are used (not shown), then the difference between COR 2 and COR 5 becomes statistically significant. Note that the information for 534 and 579°C are plotted together, and the difference in temperature for this point is likely to result in closer proximity of the point to the 1:1 line than would have been the case if the temperatures were the same. There is no significant difference between the Rb-scatterer distances for the CO_2-bearing and CO_2-free samples (Fig. 4b).

The best fit σ^2, although associated with large uncertainties, apparently decreases with temperature. This is surprising because σ^2 measures disorder, which is expected to increase with increasing temperature, as observed by Fulton et al., (1996). It is also a concern because σ^2 is correlated with n, the number of nearest neighbours, so unrealistic trends in σ^2 could cause artefacts in the results for n . It was for this reason that fits that maximised σ^2, within

the limits of acceptable residual diagnostics, were tried. Results of this work (not shown) produced similar values for the fit parameters to the original fit, and σ^2 was still found to decrease with temperature, although to a lesser extent; values for COR 2 decreased from 0.032 at room temperature to 0.027 at 534°C, and values for COR 2 decreased from 0.034 at room temperature to 0.023 at 579°C. Uncertainties on σ^2 were not constrained because this parameter was set during the fitting process. The implications of observed trends in σ^2 are discussed further below.

4.3 Br XAFS

The Br XAFS spectra (Fig.5) are lower quality than those for Rb because it was not possible to normalise these spectra to the signal from another inclusion component. Noise from movement of the bubble and small stage vibrations therefore significantly decreased the signal to noise ratio. Nevertheless, acceptable XANES spectra (Figs 5a,b, and c) were obtained and k^2 Chi(k) oscillations were visible up to a k value of around 5 or 6 (Fig. 5d, e, f). Room temperature Br XANES from CO_2-bearing inclusions show a pre-edge peak which is absent in spectra from CO_2-free inclusions (e.g. Fig. 6) but this disappeared at temperatures greater than 180°C. Comparison of the Br standard spectra (Fig. 6, Table 3) with those for the samples suggests that samples at temperatures greater than 178°C contain Br in a comparable structural environment to that of Br in an aqueous RbBr solution at room temperature, where RbBr is fully dissociated. The Br edge position (Table 3) did not vary significantly as a function of temperature or solvent composition. Peak position varied slightly but systematically with increasing temperature for both CO_2-bearing and CO_2-free inclusions, but the magnitude of the change was small (< 0.5 eV). There was no observable change in peak shape with changing temperature or solvent composition (Figs 5a,b, and c).

k^2 chi(k) oscillations showed some decrease in amplitude with increasing temperature, consistent with that observed for Rb, but the position of the oscillations was insensitive to temperature and solvent composition (Figs 5d,e,f). Further quantitative analysis of these spectra was not performed as the uncertainties would have been so large that comparisons

between the two samples would have been meaningless. However, it is possible to infer a qualitative decrease in co-ordination number from the reduction in amplitude of the chi(k).

4.4 Forward modelling

Forward modelling (Fig. 7) shows that significant changes in the degree of ion-pairing can occur without a large effect on the predicted chi(R) spectra for Rb. The model that specifies Rb surrounded by 6 oxygens (model 1) is qualitatively similar to those for other models, which include up to 66% Br. Models for which O and Br neighbours are specified to be at the same distance (2.93 Å) from the co-ordinating Rb ion are less sensitive to anion identity than those for which the Rb-Br distance is, more realistically, set to 3.4 Å.

EXAFS fitting to the model spectra using a theory that involved six oxygens at 2.93 Å produced satisfactory fits, that is, the R factor was less than 0.05, for up to 50% Br neighbours when the Br neighbours were at the same distance as the O ions, and for up to 40% Br neighbours when the Br were at 3.4 Å, which reflects the larger ion size of the Br ion. Thus, the EXAFS data provided here does not identify the co-ordinating anion for Rb unambiguously.

5 DISCUSSION

5.1 Validation of SFLINC methods

An important aspect of this study is the validation of SFLINCs as sample vessels for EXAFS measurements on fluids at high pressure and temperatures. The appeal of SFLINCs for this type of study is that high densities and CO_2 contents are more accessible than for diamond anvil cell experiments, and the preparation method is less prone to contamination than methods that use complex sample-holding apparatus, but data quality has previously been inferior to cell-hosted experiments. The SFLINCs are sufficiently large for synchrotron analysis, and

are larger than those previously reported for corundum-hosted H_2O-CO_2 SFLINCs (Frost and Wood, 1997). This is attributed to the presence of the salt in the solutions, as salts are known to enhance Al solubility, possibly via the formation of mixed cation complexes (e.g. Newton and Manning, 2006). EXAFS spectra from the SFLINCS are worse than the best from hydrothermal and diamond anvil type experiments (e.g. Mayanovic et al., 1999; Mayanovic et al., 2001; Simonet et al., 2002). Better SFLINCS are obtained using the 9mm Ag capsules than in the 5mm Pt capsules. This is attributed to the larger fluid:rock ratio that was possible in the larger capsules. However, Rb EXAFS spectra from either method are sufficiently good for EXAFS analysis after normalisation. The quality of the Br data is not good enough for EXAFS analysis, so the incorporation of a small quantity of an element that does not complex with Br and with a lower atomic number than Br, such as Ge, would allow normalisation and is recommended to improve the quality of Br spectra in future experiments. Acquisition of additional scans may also reduce noise and increase the level of detail provided by the results.

5.2 Non-unique model solutions

The forward modelling exercise shows that the chi(R) spectra are relatively insensitive to the introduction of up to 40% Br into the first coordination shell. Thus, limited ion-pairing is difficult to distinguish from changes in the number of waters of hydration. The results of the EXAFS fitting are therefore non-unique, and alternative models that involve ion-pairs could also fit the data. For this reason, subsequent discussion refers to the total number of well-ordered nearest neighbours, without assumption of their identity.

A strategy that might be able to distinguish between ion dehydration and the formation of ion-pairs would be to compare spectra for a range of Rb halides, e.g. RbBr, RbCl, and RbF. Differences between the Rb spectra would unequivocally indicate involvement of cation-anion interactions, as the bare solvated ion in solution should be identical in all three cases. A similar approach was taken by Ferlat et al., (2002), who compared spectra from Br in RbBr, KBr and CsBr solutions at 450°C and 4.5 MPa. Significant differences were not observed in

the original study, although it is not clear that ion-pairing would have been detected, even if present because of the noise present in the supercritical spectra. Additionally, such effects for Br might be easier to detect, because there is a greater difference between Br-O and Br-Rb bondlengths and strengths.

5.3 Comparison with previous work

Results for the room temperature standard and trends of the EXAFS fit results for Rb-O distances and Rb nearest neighbour numbers are comparable to those from previous work (compare Tables 2 and 4). The reduction in the amplitude of chi(k) with increasing temperature for Br is consistent with previous work (e.g. Wallen et al., 1997; Ferlat et al., 2001; Mayanovic et al., 2001). This reduction has been interpreted to record ion dehydration (Wallen et al., 1997; Ferlat et al., 2001) or increasing structural disorder in the hydration shell (Ferlat et al., 2001), but data acquired by this study cannot be used to distinguish between these hypotheses. The results are therefore used to infer loss of well-ordered waters of hydration. The term 'well-ordered' is used because water molecules in the first hydration shell with a high degree of structural disorder would not contribute much to the chi(R) signal and could be effectively invisible for the purposes of this technique (Ferlat et al. 2001).

The decrease in σ^2 for Rb is different to trends in σ^2 recorded by the previous study of RbBr (Fulton et al., 1996), and cannot be attributed to correlations between the fit parameters because unacceptable fits are obtained if σ^2 is forced to increase. There are a number of factors which may help to explain this discrepancy. First is the density of the experiments. The density of the experiments of Fulton et al. (1996) decreased as temperature increased and this would have enhanced the extent of increases in disorder with increasing temperature. Density in the experiments reported here is fixed by the fixed volume of the fluid inclusion, so increases in disorder would be expected to be less. The second is that the decrease in the number of nearest neighbours may be associated with an increase in the degree of ordering of those neighbours, simply because there are less of them and thus, the effective charge contributed to each bond becomes greater. The third reason relates to the

absolute pressure of the fluids under observation; the fluids observed by Fulton et al. were at pressures less than 633 bars, whereas those used for this study were at pressures up to a factor of four higher. Such high pressures may damp the increases in thermal disorder that would have been recorded by σ^2. Other studies have also noted small or negligible increases in σ^2 with temperature, e.g. Fulton et al. (2006).

5.4 Effects of CO_2 on Rb speciation

The EXAFS results suggest a loss of well-ordered nearest neighbours from the first Rb shell with increasing temperature, and bond length contraction for COR 2 (Table 2; Fig. 4). The bond length contraction for Rb-x for COR 2 records an increase in Coulombic forces as the dielectric constant decreases and the ability of the solution to screen charge between ions is reduced.

The fit parameters remain relatively constant once supercritical conditions have been reached. This result is consistent with results for other ionic species (e.g. Simonet et al., 2002). The more drastic changes at lower temperatures are attributed to the steep gradients in fluid properties such as dielectric constant and compressibility that exist under near-critical conditions (e.g. Helgeson and Kirkham, 1974). Results do, however, change with pressure and temperature above the critical point, even at the fixed density imposed by the SFLINC method. This contradicts the proposal (Pfund et al., 1994) that the number of nearest neighbours is proportional to the fluid density.

The results indicate that fit values for the numbers of well-ordered nearest neighbours and Rb-x distances are sensitive to the CO_2 concentration, although this is strictly speaking within the limits of uncertainties of the fits. However, the relative positions of the points is likely to be more reliable than their absolute positions, so the conclusion that there is a difference between the results for the CO_2-bearing and CO_2-free samples is likely to be robust. The results are also supported by the consensus between results from the different fitting strategies.

An additional check on the significance of the difference in n between the CO_2-bearing and

CO_2-free solutions was performed via a comparison of changes in the calculated dielectric constant for the SFLINC solutions with fit values of n for COR 2 and COR 5 (Fig. 8a). Dielectric constants were calculated with the formulation of Archer and Wang (1990) and a modified form of the Kirkwood equation (Kirkwood, 1939). The contribution of RbBr to the dielectric constant is not included in this calculation, but salt concentrations in the two samples are similar so this omission is unlikely to have a significant effect. If temperature and X(CO_2)-driven changes in bulk solution dielectric constant affect solvation in the CO_2-free and CO_2-bearing inclusions equally then points from the two types of inclusions would lie on a single trend. If temperature were the only determinant of n then the points would lie on parallel trends, with points taken at the same temperature having the same n. The results are consistent with the former scenario, and suggest that it may be possible to predict X(CO_2)-driven effects on solvation from calculated changes in dielectric constant. Rb-nearest neighbour distances were also plotted against dielectric constant (Fig. 8b) and an apparent decrease and increase in values can be seen. However, the uncertainties on this parameter are sufficiently large that this trend cannot be stated conclusively to be significant or informative.

5.5 Geological implications

Dissolution and transport of the components of mineral phases by aqueous fluids is ubiquitous in metamorphic environments, and is of particular interest when the fluids are associated with ore formation. Examples include the sodium metasomatism that is often observed at gold deposits (e.g. Albino, 1995), and potassium metasomatism associated with granulite metamorphism (e.g. Todd and Evans, 1994).

Prediction of the capacity of fluids to dissolve and precipitate material utilise thermodynamic models, which incorporate activity coefficients to quantify the deviation of solute and solvent properties from ideal behaviour. The vast majority of these models (e.g. Helgeson et al., 1983; Pitzer and Simonson, 1986; Gibert et al., 1992; Sverjensky et al., 1997; Akinviev and Zotov, 1999; Evans and Powell, 2006, 2007) use some modification of the Debye-Huckel

equation, which includes the dielectric constant. However, few models incorporate solvent-related effects on dielectric constant, and this could induce systematic errors into calculations on solutions where non-aqueous solvent components are significant. The implications of this possibility have been discussed by Walther (1992); the results of this study demonstrate the effects of solvent composition experimentally for the first time. Additionally, calculated thermodynamic properties for solutes implicitly incorporate the thermodynamic effects of waters of hydration. If the number of waters of hydration varies with solvent composition then there may also be systematic errors in thermodynamic properties with consequent effects for calculated mineral stabilities and solution compositions.

However, realistically, the errors introduced by poor conceptual models for fluid structures are likely to be smaller than, or comparable to, the numerous other uncertainties involved in thermodynamic calculations on dissolved aqueous species in mixed solvent, high ionic strength solutions. Nevertheless, the concepts discussed here may be useful in consideration of supercritical fluid-bearing geological environments, even if quantitative calculations are not yet possible.

6 CONCLUSIONS

Corundum is an excellent host for fluid inclusions, and allows synchrotron measurements of CO_2-bearing fluids to be made at pressures up to 0.26 GPa without significant beam- or heating-induced damage to the inclusions. SFLINCs hosted by corundum produce EXAFS data sufficiently good to derive first shell information up to k values of around 7 $Å^{-1}$. However, the modelling results may not provide a unique solution to the solute speciation; forward modelling shows that it is difficult to distinguish between ion-pairing and a decrease in the number of nearest oxyen neighbours.

Fit results for Rb in the SFLINCS suggest that the number of well-ordered nearest neighbours is smaller for CO_2-bearing inclusions than for CO_2-free inclusions by 15-25%. Differences in the number of nearest neighbours can be related to changes in dielectric constant, and it may be possible to predict such changes from this parameter. Such a strategy would

be useful because solvent-induced effects on the thermodynamics of CO_2-bearing solutions are not accounted for in the majority of current thermodynamic models. The decrease in nearest neighbour numbers is accompanied by a contraction in the Rb-O bondlength for the CO_2-free sample but is not observed for the CO_2-bearing sample. Results for Br are limited but show a decrease in the amplitude of chi(k) oscillations with increasing temperature, consistent with a decrease in the numbers of waters of solvation with temperature that has been inferred from previous work.

Further work is necessary to constrain the systematics of Br solvation, to distinguish between ion-pairing and solute dehydration, and to investigate the nature of local variations in solvent properties under supercritical conditions.

Acknowledgments. Mike Shelley is thanked for silver oxalate synthesis and help with many other aspects of the work. Matt Newville is thanked for help with early investigations of quartz-hosted fluid inclusions and discussion of fluid properties. This work was performed with support from the Australian Synchrotron Research Program (ASRP), which is funded by the Commonwealth of Australia under the Major National Research Facilities Program. PNC/XOR facilities at the Advanced Photon Source, and research at these facilities, are supported by the US Department of Energy - Basic Energy Sciences, a major facilities access grant from NSERC, the University of Washington, Simon Fraser University and the Advanced Photon Source. Use of the Advanced Photon Source is also supported by the U. S. Department of Energy, Office of Science, Office of Basic Energy Sciences, under Contract DE-AC02-06CH11357. Denis Testemales and three anonymous reviewers are thanked for detailed and perceptive comments on an earlier version of this paper. David Cole and Frank Podosek are thanked for editorial handling.

REFERENCES

Akinfiev, N. and Zotov, A. (1999). Thermodynamic description of equilibria in mixed fluids (H_2O- non-polar gas) over a wide range of temperature (25-700 Degrees C) and pressure (1-5000 Bars). *Geochim. Cosmochim. Acta* **63**, 2025-2041.

Albino, G. V. (1995). Sodium metasomatism along the Melones fault zone, Sierra-Nevada foothills, California, USA. *Min. Mag.* **59**, 383-399.

Archer, D. G. and Wang, P. M. (1990). The dielectric-constant of water and Debye-Huckel limiting law slopes. *J. Phys. Chem. Ref. Data* **19**, 371-411.

Baker, T. (2002). Emplacement depth and carbon dioxide-rich fluid inclusions in intrusion-related gold deposits. *Econ. Geol.* **97**, 1111-1117.

Bowers, T. S. and Helgeson, H. C. (1985). Fortran programs for generating fluid inclusion isochores and fugacity coefficients for the system H_2O-CO_2-NaCl at high-pressures and temperatures. *Comput. Geosci.* **11**, 203-213.

Brown, P. E. and Hagemann, S. G. (1995). Macflincor and Its application to fluids in Archean lode-gold deposits. *Geochim. Cosmochim. Acta* **59**, 3943-3952.

Brown, P. E. and Lamb, W. M. (1989). P-V-T properties of fluids in the system $H_2O \pm CO_2 \pm$NaCl. *Geochim. Cosmochim. Acta* **53**, 1209-1221.

Butterfield, D. A., McDuff, R. E., Mottl, M. J., Lilley, M. D., Lupton, J. E., and Massoth, G. J. (1994). Gradients in the composition of hydrothermal fluids from the Endeavor Segment Vent Field - phase-separation and brine loss. *J. Geophys. Res. B: Solid Earth* **99**, 9561-9583.

Caracausi, A., Ditta, M., Italiano, F., Longo, M., Nuccio, P. M., and Paonita, A. (2005). Changes in fluid geochemistry and physico-chemical conditions of geothermal systems caused by magmatic input: The recent abrupt outgassing off the island of Panarea (Aeolian Islands, Italy). *Geochim. Cosmochim. Acta* **69**, 3045-3059.

572 Duan, Z., Moller, N., and Weare, J. (1995). Equation of state for the NaCl-H_2O-CO_2 sys-
573 tem: prediction of phase equilibria and volumetric properties. *Geochim. Cosmochim.*
574 *Acta* **59**, 2869-2882.

575 Duan, Z. H., Moller, N., and Weare, J. H. (2003). Equations of state for the NaCl-H_2O-
576 CH_4 system and the NaCl-H_2O-CO_2-CH_4 system: Phase equilibria and volumetric
577 properties above 573 K. *Geochim. Cosmochim. Acta* **67**, 671-680.

578 Evans, K. and Powell, R. (2006). A method for activity calculations in saline and mixed
579 solvent solutions at elevated temperature and pressure: A framework for geological
580 phase equilibria calculations. *Geochim. Cosmochim. Acta* **70**, 5488-5506.

581 Evans, K. A., Mavrogenes, J., and Newville, M. (2007). The effect of CO_2 on the speciation
582 of bromine in low-temperature geological solutions: an XANES study. *J. Synch. Rad.*
583 **14**, 219-226.

584 Evans, K. A. and Powell, R. (2007). DES-code: A metacode to aid calculation of the chem-
585 ical potential of aqueous solutions at elevated temperatures and pressures. *Comput.*
586 *Geosci.* **33**, 789-807.

587 Ferlat, G., San Miguel, A., Jal, J. F., Soetens, J. C., Bopp, P. A., Daniel, I., Guillot, S.,
588 Hazeman, J. L., and Argoud, R. (2001). Hydration of the bromine ion in a supercritical
589 1 : 1 aqueous electrolyte. *Phys. Rev. B* **6313**.

590 Ferlat, G., San Miguel, A., Jal, J. F., Soetens, J. C., Bopp, P. A., Hazeman, J. L., Testemale,
591 D., and Daniel, I. (2002). The quest for ion-pairing in supercritical aqueous electrolytes.
592 *J. Mol. Liq.* **101**, 127-136.

593 Ferry, J. M. (1994). Overview of the petrological record of fluid flow during regional meta-
594 morphism in northern New England. *Am. J. Sci.* **294**, 905-988.

595 Frenkel, A. I., Stern, E. A., Qian, M., and Newville, M. (1993). Multiple-scattering X-Ray-
596 absorption fine-structure analysis and thermal-expansion of alkali-halides. *Phys. Rev.*
597 *B* **48**, 12449-12458.

598 Frost, D. J. and Wood, B. J. (1997). Experimental measurements of the properties of H_2O-
599 CO_2 mixtures at high pressures and temperatures. *Geochim. Cosmochim. Acta* **61**,
600 3301-3309.

601 Fulton, J. L., Pfund, D. M., Wallen, S. L., Newville, M., Stern, E. A., and Ma, Y. (1996).
602 Rubidium ion hydration in ambient and supercritical water. *J. Chem. Phys.* **105**,
603 2161-2166.

604 Gibert, F., Moine, B., Schott, J., and Dandurand, J.-L. (1992). Modelling of the trans-
605 port and deposition of tungsten in the scheelite-bearing calc-silicate gneisses of the
606 Montagne Noire, France. *Contrib. Mineral. Petrol.* **112**, 371-384.

607 Heald, S. M., Stern, E. A., Brewe, D., Gordon, R. A., Crozier, D., Jiang, D., and Cross,
608 J. (2001). XAFS at the Pacific Northwest Consortium-Collaborative Access Team
609 undulator beamline. *J. Synch. Rad.* **8**, 342-344.

610 Gordon, R.A., Crozier, E.D., Jiang, D.-T., Monchesky, T.L. and Heinrich, B., 2000. Dis-
611 torted iron films on GaAs(001)-(4x6). Physical Review B, 62: 2151-2157.

612 Helgeson, H. C. and Kirkham, D. H. (1974). Theoretical prediction of the thermodynamic
613 behaviour of aqueous elctrolytes at high pressures and temperatures: I. Summary of the
614 thermodynamic/electrostatic properties of the solvent. *Am. J. Sci.* **274**, 1089-1198.

615 Helgeson, H. C., Kirkham, D. H., and Flowers, G. C. (1981). Theoretical prediction of the
616 thermodynamic behaviour of aqueous electrolytes at high pressures and termperatures:
617 IV Calculation of activity coefficients, osmotic coefficients, and apparent molal and
618 standard and relative partial molal properties to 600 degrees C and 5 kbar. *Am. J.*
619 *Sci.* **281**, 1259-1516.

620 Holness, M. B. and Graham, C. M. (1995). P-T-X effects on equilibrium carbonate-H_2O-
621 CO_2-NaCl dihedral angles - constraints on carbonate permeability and the role of
622 deformation. *Contrib. Mineral. Petrol.* **119**, 301-313.

623 Kirkwood, J. G. (1939). The dielectric polarization of polar liquids. *J. Phys. Chem.* **7**,
624 911-919.

Mavrogenes, J. A., Berry, A. J., Newville, M., and Sutton, S. R. (2002). Copper speciation in vapor-phase fluid inclusions from the Mole Granite, Australia. *Am. Min.* **87**, 1360-1364.

Mavrogenes, J. A., Bodnar, R. J., Anderson, A. J., Bajt, S., Sutton, S. R., and Rivers, M. L. (1995). Assessment of the uncertainties and limitations of quantitative elemental analysis of individual fluid inclusions using synchrotron X-ray-fluorescence (Sw). *Geochim. Cosmochim. Acta* **59**, 3987-3995.

Mayanovic, R. A., Anderson, A. J., Bassett, W. A., and Chou, I. M. (1999). XAFS measurements on zinc chloride aqueous solutions from ambient to supercritical conditions using the diamond anvil cell. *J. Synch. Rad.* **6**, 195-197.

Mayanovic, R. A., Anderson, A. J., Bassett, W. A., and Chou, I. M. (2001). Hydrogen bond breaking in aqueous solutions near the critical point. *Chemical Physics Letters* **336**, 212-218.

Newton, R. C., Aranovich, L. Y., Hansen, E. C., and Vandenheuvel, B. A. (1998). Hypersaline fluids in Precambrian deep-crustal metamorphism. *Precamb. Res.* **91**, 41-63.

Newton, R. C. and Manning, C. E. (2000). Quartz solubility in H_2O-NaCl and H_2O-CO_2 solutions at deep crust-upper mantle pressures and temperatures: 2-15 kbar and 500-900oC. *Geochim. Cosmochim. Acta* **64**, 2993-3005.

Newton, R. C. and Manning, C. E. (2006). Solubilities of corundum, wollastonite and quartz in H_2O-NaCl solutions at 800 degrees C and 10 kbar: Interaction of simple minerals with brines at high pressure and temperature. *Geochim. Cosmochim. Acta* **70**, 5571-5582.

Newville, M. (2001). IFEFFIT: interactive EXAFS analysis and FEFF fitting. *J. Synch. Rad.* **8**, 322-324.

Newville, M., Fulton, J. L., Pfund, D. M., Wallen, S. L., Stern, E. A., and Ma, Y. (1997). XAFS measurements of Rb-O bonds in ambient and supercritical water. *J. Physique.* **7**, 1007-1008.

652 Pfund, D. M., Darab, J. G., Fulton, J. L., and Ma, Y. J. (1994). An XAFS Study of
653 strontium ions and krypton in supercritical water. *J. Phys. Chem.* **98**, 13102-13107.

654 Phillips, G. N. and Evans, K. A. (2004). Role of CO_2 in the formation of gold deposits.
655 *Nature* **429**, 860-863.

656 Phillips, G. N. and Powell, R. (1993). Link between gold provinces. *Econ. Geol.* **88**,
657 1084-1098.

658 Pitzer, K. S. and Simonson, J. M. (1986). Thermodynamics of multicomponent, miscible,
659 ionic systems - theory and equations. *J. Phys. Chem.* **90**, 3005-3009.

660 Ravel, B. and Newville, M. (2005). ATHENA, ARTEMIS, HEPHAESTUS: data analysis
661 for X-ray absorption spectroscopy using IFEFFIT. *J. Synch. Rad.* **12**, 537-541.

662 Seward, T. M., Henderson, C. M. B., Charnock, J. M., and Driesner, T. (1999). An EXAFS
663 study of solvation and ion pairing in aqueous strontium solutions to 300 degrees C.
664 *Geochim. Cosmochim. Acta* **63**, 2409-2418.

665 Shelton, K. L. and Orville, P. M. (1980). Formation of synthetic fluid inclusions in natural
666 quartz. *Am. Min.* **65**, 1233-1236.

667 Shmulovich, K., Graham, C., and Yardley, B. (2001). Quartz, albite and diopside solubili-
668 ties in H_2O-NaCl and H_2O-CO_2 fluids at 0.5-0.9 GPa. *Contrib. Mineral. Petrol.* **141**,
669 95-108.

670 Shmulovich, K. I. and Graham, C. M. (1999). An experimental study of phase equilibria
671 in the system H_2O-CO_2-NaCl at 800°C and 9 kbar. *Contrib. Mineral. Petrol.* **136**,
672 247-257.

673 Simonet, V., Calzavara, Y., Hazemann, J. L., Argoud, R., Geaymond, O., and Raoux, D.
674 (2002). X-ray absorption spectroscopy studies of ionic association in aqueous solutions
675 of zinc bromide from normal to critical conditions. *J. Chem. Phys.* **117**, 2771-2781.

676 Sterner, S. M. and Bodnar, R. J. (1984). Synthetic fluid inclusions in natural quartz
677 .1. compositional types synthesized and applications to experimental geochemistry.
678 *Geochim. Cosmochim. Acta* **48**, 2659-2668.

679 Sverjensky, D. A., Shock, E. L., and Helgeson, H. C. (1997). Prediction of the thermody-
680 namic properties of aqueous metal complexes to 1000 degrees C and 5 kB. *Geochim.*
681 *Cosmochim. Acta* **61**, 1359-1412.

682 Thebaud, N., Philippot, P., Rey, P., and Cauzid, J. (2006). Composition and origin of flu-
683 ids associated with lode gold deposits in a Mesoarchean greenstone belt (Warrawoona
684 Syncline, Pilbara Craton, Western Australia) using synchrotron radiation X-ray fluo-
685 rescence. *Contrib. Mineral. Petrol.* **152**, 485-503.

686 Todd, C. S. and Evans, B. W. (1994). Properties of CO_2-induced dehydration of amphibo-
687 lite. *J. Pet.* **35**, 1213-1239.

688 Wallen, S. L., Palmer, B. J., Pfund, D. M., Fulton, J. L., Newville, M., Ma, Y. J., and Stern,
689 E. A. (1997). Hydration of bromide ion in supercritical water: an X-Ray Absorption
690 Fine Structure and molecular dynamics study. *J. Phys. Chem.* **101**, 9632-9640.

691 Walther, J.V., 1992. Ionic association in H_2O and CO_2 fluids. J. Met. Geol., 10: 789-797.

692 Wark, D. A. and Watson, E. B. (2002). Grain-scale channelization of pores due to gradients
693 in temperature or composition of intergranular fluid or melt. *J. Geophys. Res. B: Solid*
694 *Earth* **107**.

695 Wyckoff (1963). *Crystal Structures.* John Wiley and Sons, New York.

696 Zelyanskii, A. V., Zhukova, L. V., and Kitaev, G. A. (2001). Solubility of AgCl and AgBr
697 in HCl and HBr. *Inorganic Materials* **37**, 523-526.

Table 1: Inclusion characteristics

Parameter	COR 2	COR 5
$X(RbBr)_{intended}$	0.01	0.08
$X(CO_2)_{intended}$	0	0.08
$Density_{intended}$ (g cm^{-3})	0.8	0.8
Pressure of run (GPa)	0.8	0.8
Temperature of run (°C)	900	800
T(total homogenisation) (°C)	385 (25)[1]	384.9 (3.3)[1]
T(final melting) (°C)	-12.1 (2.9)[1]	-0.7 (0.4)[1]
T(CO_2 homogenisation)(°C)	n/a	28.8 (0.6)[1]
$X(salt)_{calculated}$	0.05 (0.007)[1,2]	0.05 (0.004)[1,2]
RbBr $molality_{calculated}$	2.92 (0.4)[1,2]	3.2 (0.25)[1,2]
$X(CO_2)_{calculated}$	n/a	0.08 (0.03)[1,2]
CO_2 $molality_{calculated}$	n/a	5.1(1.9)[1,2]
$Density_{calculated}$ (g cm^{-3})	0.82 (0.11)[1,2]	0.79 (0.09)[1,2]

[1]Figures in brackets are one standard deviation on measured or calculated parameters.
[2]Uncertainties on calculated parameters are propagated from measured uncertainties

Table 2: IFEFFIT modelling results for Rb

Sample	T (°C)	P(GPa)	N	R($\mathring{A}$)	$\sigma^2(\mathring{A}^2)$	$c3$	Rfactor
COR 2	20	<0.05	6.0(17/6)	2.93(4/2)	0.032(9/5)	0.010(3/1)	0.014
COR 2	178	<0.05	4.0(8/3)	2.91(2/1)	0.027(6/3)	0.012(2/1)	0.007
COR 2	312	0.0095	2.5(3/2)	2.88(2/1)	0.019(4/2)	0.010(1/1)	0.004
COR 2	445	0.13	1.8(6/2)	2.9(4/1)	0.014(9/5)	0.013(3/1)	0.023
COR 2	534	0.25	1.4(3/1)	2.88(3/2)	0.009(6/4)	0.012(2/1)	0.013
COR 5	20	<0.05	5.8(13/5)	2.93(2/1)	0.029(7/4)	0.010(1/1)	0.010
COR 5	89	<0.05	2.4(3/2)	2.93(2/1)	0.015(4/2)	0.007(1/1)	0.006
COR 5	178	<0.05	3.2(5/3)	2.95(2/1)	0.020(5/3)	0.013(2/1)	0.006
COR 5	312	0.032	2.1(6/3)	2.94(3/2)	0.015(8/4)	0.014(2/2)	0.019
COR 5	445	0.23	1.4(4/2)	2.89(3/2)	0.011(7/5)	0.010(2/2)	0.021
COR 5	579	0.26	1.4(5/2)	2.92(4/2)	0.011(10/6)	0.014(3/2)	0.031
0.001m RbBr	20	$1x10^{-4}$	5.7(8)	2.91(2)	0.033(7)	not fit	0.019
2m RbBr in 0.8m $NaHCO_3$	20	$1x10^{-4}$	4.3(5)	2.91(2)	0.017(5)	not fit	0.016

T: Temperature
N: Number of nearest neighbours
R: Rb-O distance
σ^2: Mean square relative displacement
$c3$: Third cumulant
First figure in brackets is one standard deviation on the last significant figure calculated by Artemis, second figure is one standard deviation on the last significant figure calculated after Gordon et al. (2000)

Table 3: XANES characteristics for Br spectra

Sample	Temperature	Edge (eV)[1]	Peak (eV)[1]
COR 2	20	13477.1	13480.2
COR 2	178	13476.5	13480.4
COR 2	312	13476.5	13480.4
COR 2	445	13476.5	13480.4
COR 2	534	13476.5	13480.6
COR 5	20	13478.4	13482
COR 5	178	13477	13481.3
COR 5	312	13477	13481.2
COR 5	445	13476.5	13480.9
0.001m Br in H_2O	20	13476.1	13480
RbBr solid	20	13477.6	13479
2m RbBr in 0.8m $NaHCO_3$	20	13476	13479.6

[1]Relative uncertainties are ± 0.5 eV

Table 4: Comparison with previous work for Rb

Study	P (MPa)	T(°C)	M(salt)	n_O	r_{Rb-O} ($\AA$)
Fulton et al. 1996	1	rt	0.5	5.6	2.93
Fulton et al. 1996	38.9	178	0.5	4.4	2.87
Fulton et al. 1996	38.9	365	0.5	3.5	2.83
Fulton et al. 1996	38.3	424	0.5	3.4	2.82
Fulton et al. 1996	38.6	424	0.5	3.6	2.79
Fulton et al. 1996	63.3	424	0.5	3.9	2.81

P: Pressure
T: Temperature
M: Molality of salt
N: Number of oxygen nearest neighbours
r: Rb-O distance

FIGURE CAPTIONS

Figure 1. Photomicrographs of the fluid inclusions investigated for this study. Scale bar is 20 microns. The black lozenge in a is the approximate size of the synchrotron beam. a: COR 2 (CO_2-free) before synchrotron analysis. b: COR 5 (CO_2-bearing) before synchrotron analysis. c: COR 2 after synchrotron analysis, note damage to some near surface inclusions. d: COR 5 after synchrotron analysis.

Figure 2. Rb EXAFS spectra. a: chi(k) spectra for CO_2-free inclusions; b: chi(k) spectra for CO_2-bearing inclusions; c: chi(R) spectra for CO_2-free inclusions; d: chi(R) spectra for CO_2-bearing inclusions;

Figure 3. Fits to Rb EXAFS spectra for selected temperatures. Fits at other temperatures are similar in quality; a: magnitude of chi(R) spectra and associated fit for CO_2-free inclusion at 312°C; b: magnitude of chi(R) spectra and associated fit for CO_2-bearing inclusion at 579°C; c: real part of the chi(R) spectra and associated fit for CO_2-free inclusion at 312°C; d: real part of the chi(R) spectra and associated fit for CO_2-bearing inclusion at 579°C; e: imaginary part of the chi(R) spectra and associated fit for CO_2-free inclusion at 312°C; f:imaginary part of the chi(R) spectra and associated fit for CO_2-bearing inclusion at 579°C;

Figure 4. Results of fitting Rb EXAFS spectra. Uncertainties are calculated from the parameter values that cause a doubling of χ^2. a: Comparison between fit number of nearest neighbours for COR 2 (CO_2-free) and COR 5 (CO_2-bearing). b: Comparison of changes in bond length between COR 2 (CO_2-free) and COR 5 (CO_2-bearing).

Figure 5. Br XANES spectra. a: Comparison of XANES spectra for CO_2-free and CO_2-bearing inclusions at 178°C; b: Comparison of XANES spectra for CO_2-free and CO_2-bearing inclusions at 312°C; c: Comparison of XANES spectra for CO_2-free and CO_2-bearing inclusions at 445°C; d: Comparison of k^2 chi(k) spectra for CO_2-free and CO_2-bearing inclusions at 178°C; e: Comparison of k^2 chi(k) spectra for CO_2-free and

724 CO_2-bearing inclusions at 312°C; f: Comparison of k^2 chi(k) spectra for CO_2-free and
725 CO_2-bearing inclusions at 445°C;

726 Figure 6. Br spectra for standards:

727 Figure 7. Forward modelling results. Models 1 to 3 are very similar and indicate that
728 ion-pairing may be difficult to distinguish from ion-dehydration. Models 4 and 5 show
729 greater spectral changes;

730 Figure 8. a: Fit number of n, the number of well-ordered nearest neighbours, plotted against
731 calculated dielectric constant. Uncertainties are taken from the Artemis output; b: Fit
732 Rb-scatterer distances, plotted against calculated dielectric constant. Uncertainties
733 are taken from the Artemis output.

7 FIGURES

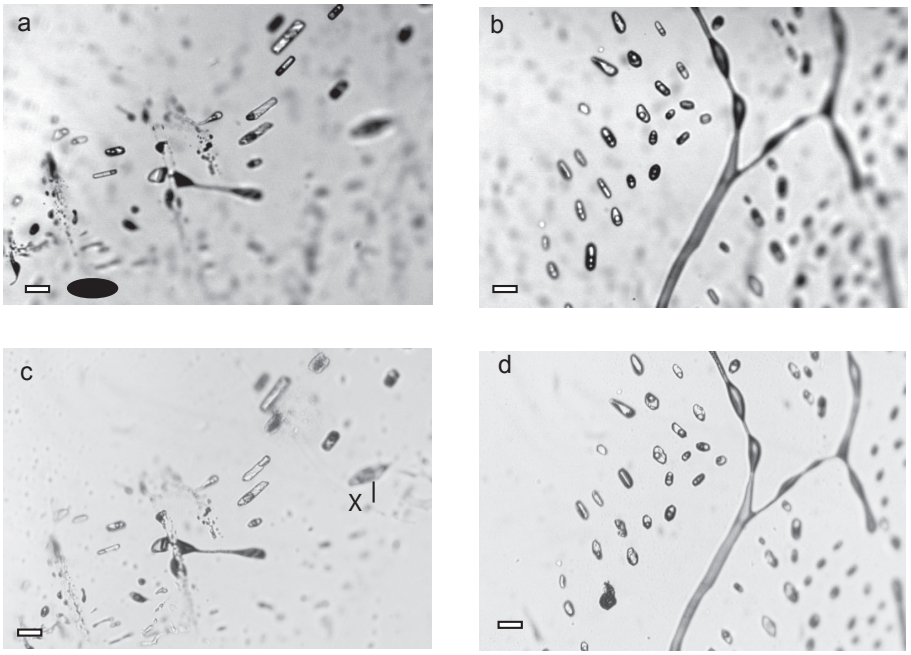

Figure 1:

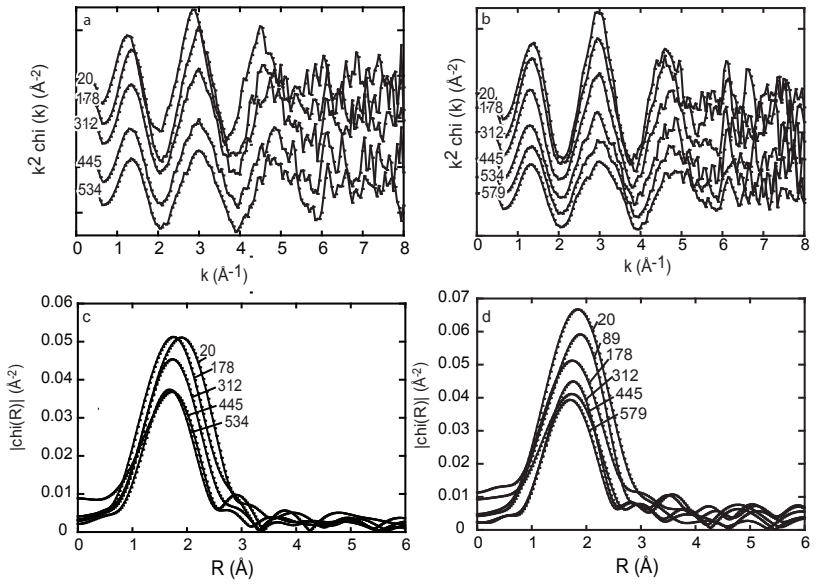
a
20
178
312
445
534
k2 chi (k) (Å-2)
k (Å-1)
b
20
178
312
445
534
579
k2 chi (k) (Å-2)
k (Å-1)
c
20
178
312
445
534
|chi(R)| (Å-2)
R (Å)
d
20
89
178
312
445
579
|chi(R)| (Å-2)
R (Å)

Figure 2:

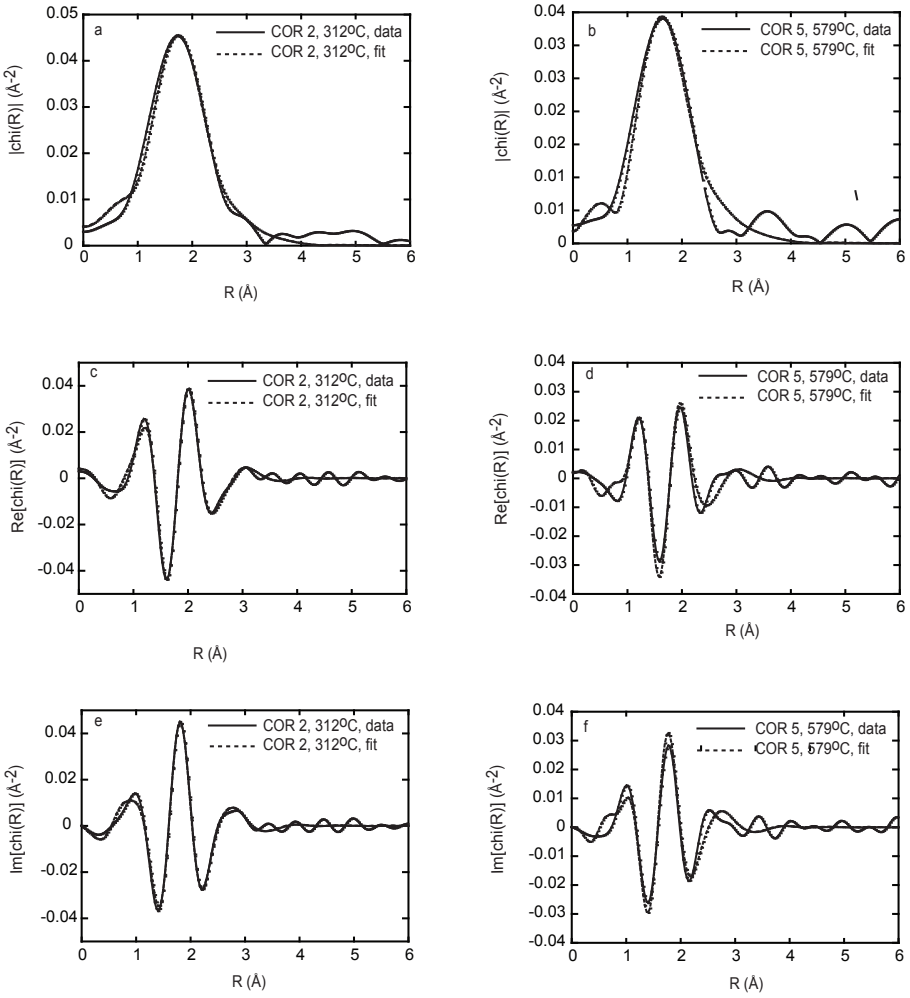
a
COR 2, 312°C, data
COR 2, 312°C, fit
|chi(R)| (Å-2)
R (Å)
b
COR 5, 579°C, data
COR 5, 579°C, fit
|chi(R)| (Å-2)
R (Å)
c
COR 2, 312°C, data
COR 2, 312°C, fit
Re[chi(R)] (Å-2)
R (Å)
d
COR 5, 579°C, data
COR 5, 579°C, fit
Re[chi(R)] (Å-2)
R (Å)
e
COR 2, 312°C, data
COR 2, 312°C, fit
Im[chi(R)] (Å-2)
R (Å)
f
COR 5, 579°C, data
COR 5, 579°C, fit
Im[chi(R)] (Å-2)
R (Å)

Figure 3:

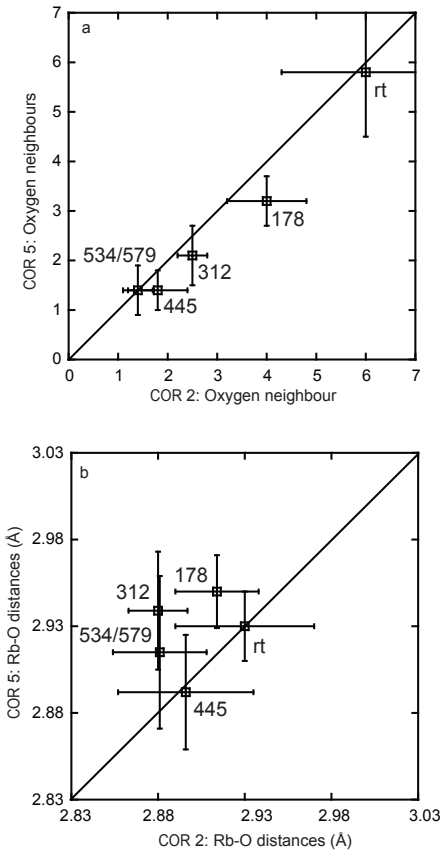
a
COR 5: Oxygen neighbours
COR 2: Oxygen neighbour
rt
178
534/579
312
445
b
COR 5: Rb-O distances (Å)
COR 2: Rb-O distances (Å)
178
312
534/579
rt
445

Figure 4:

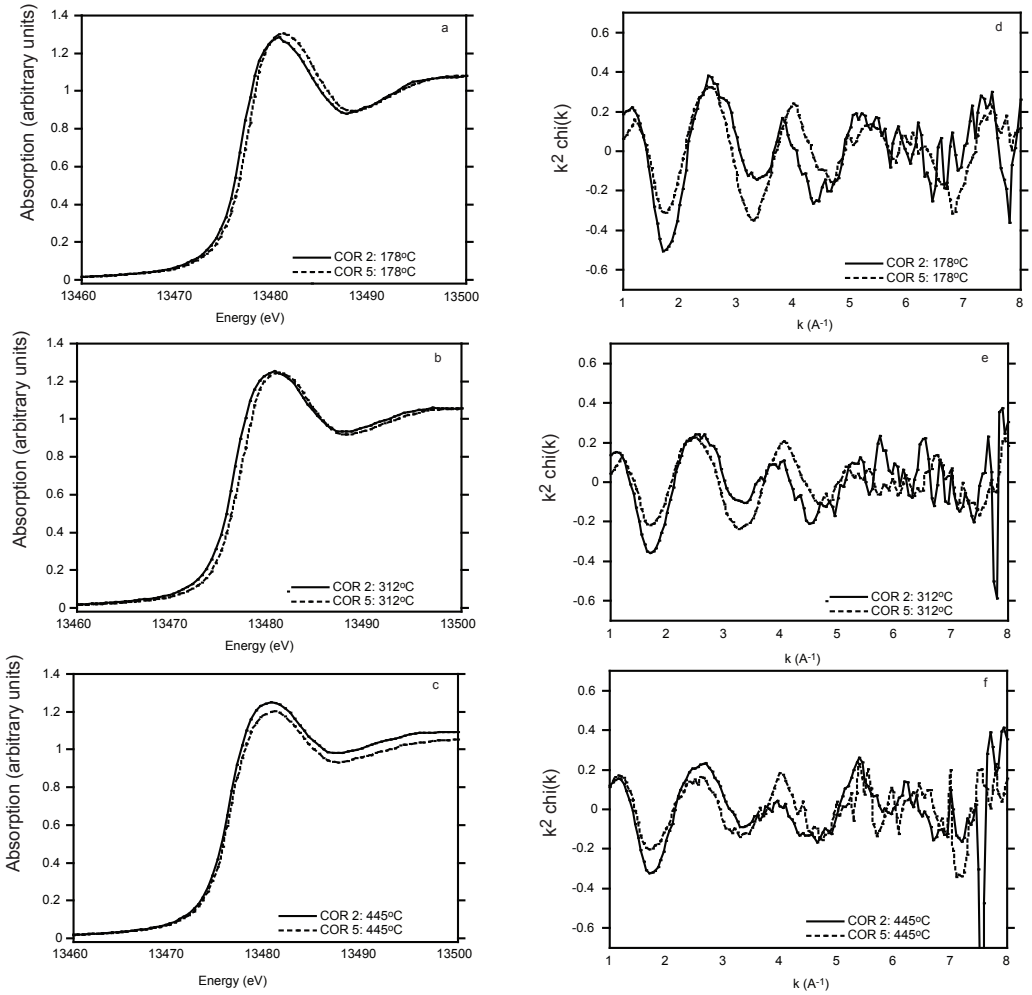
a
Absorption (arbitrary units)
Energy (eV)
COR 2: 178ºC
COR 5: 178ºC
b
COR 2: 312ºC
COR 5: 312ºC
c
COR 2: 445ºC
COR 5: 445ºC
d
k2 chi(k)
k (A-1)
e
f

Figure 5:

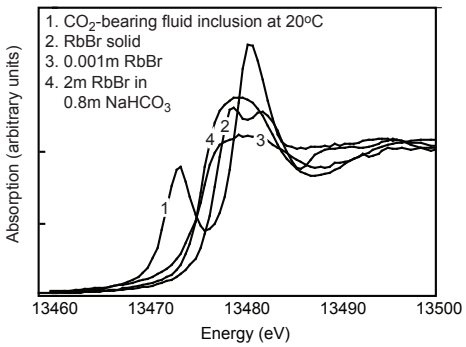
1. CO_2-bearing fluid inclusion at 20°C
2. RbBr solid
3. 0.001m RbBr
4. 2m RbBr in
0.8m $NaHCO_3$
Absorption (arbitrary units)
13460
13470
13480
13490
13500
Energy (eV)
1
2
3
4

Figure 6:

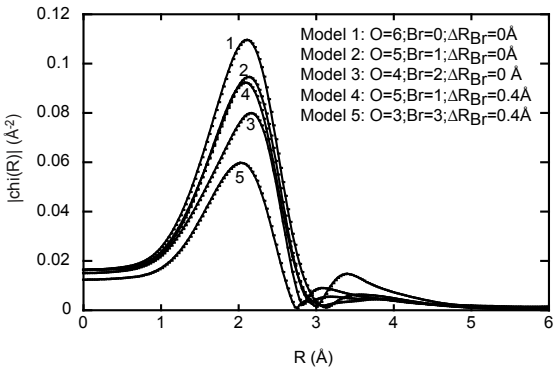
Model 1: O=6;Br=0;ΔR_Br=0Å
Model 2: O=5;Br=1;ΔR_Br=0Å
Model 3: O=4;Br=2;ΔR_Br=0 Å
Model 4: O=5;Br=1;ΔR_Br=0.4Å
Model 5: O=3;Br=3;ΔR_Br=0.4Å
|chi(R)| (Å-2)
R (Å)
0.12
0.1
0.08
0.06
0.04
0.02
0
0
1
2
3
4
5
6
1
2
4
3
5

Figure 7:

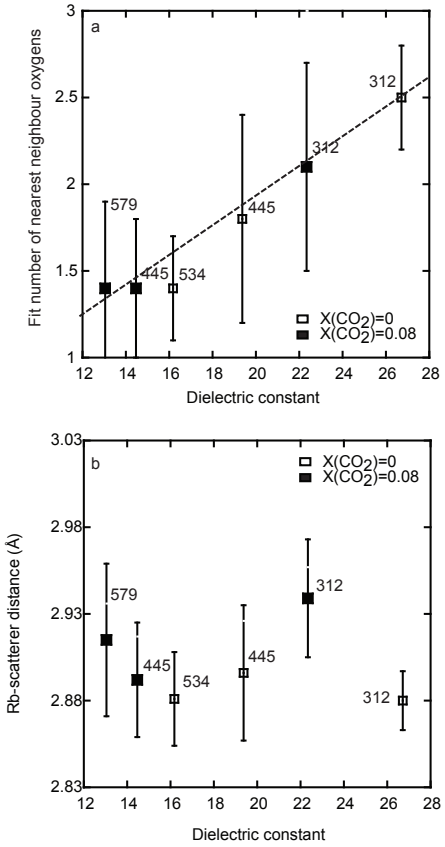
a
Fit number of nearest neighbour oxygens
Dielectric constant
X(CO2)=0
X(CO2)=0.08
579
445
534
445
312
312
b
Rb-scatterer distance (Å)
Dielectric constant
X(CO2)=0
X(CO2)=0.08
579
445
534
445
312
312

Figure 8: